Figure S1

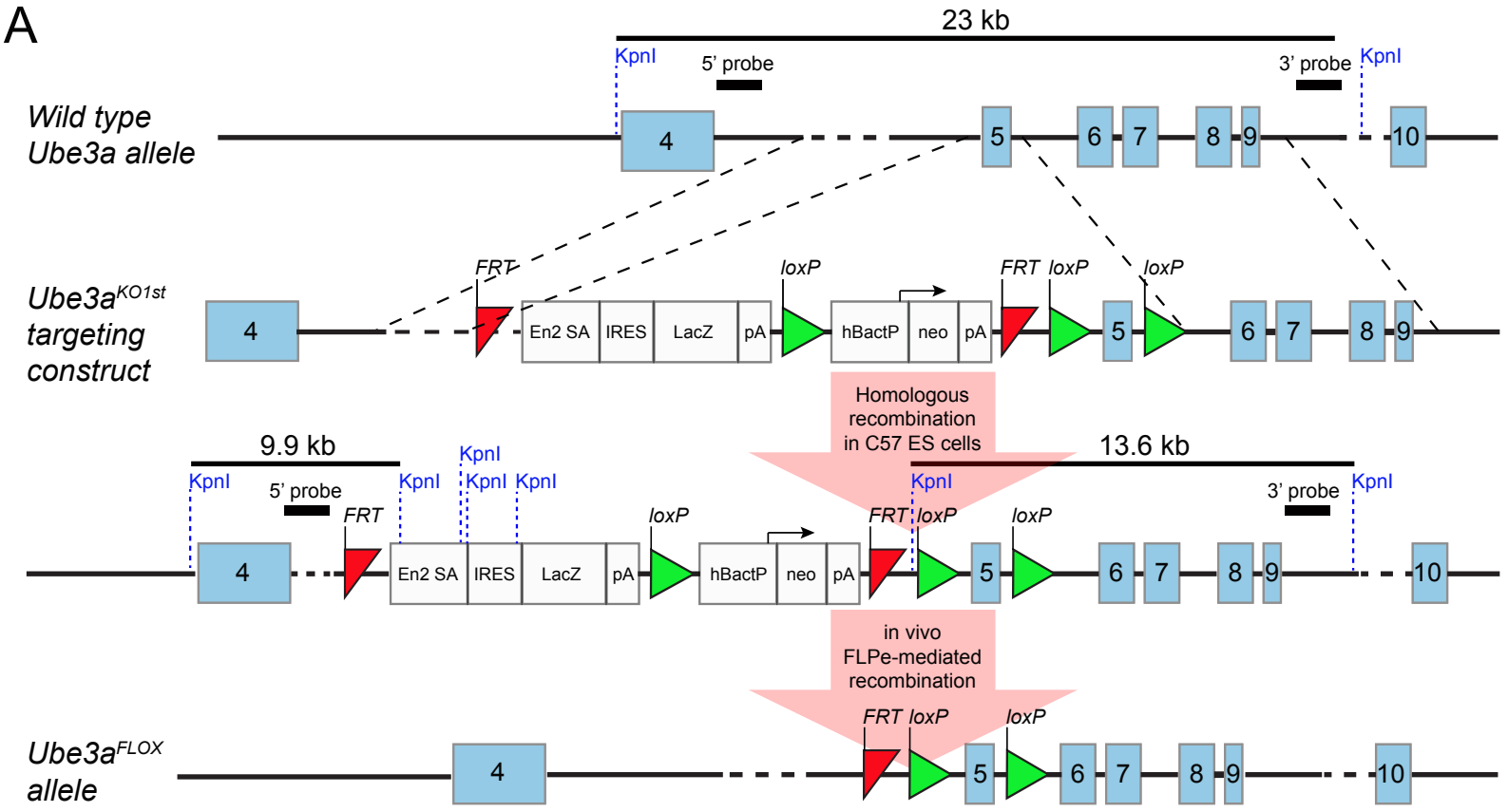

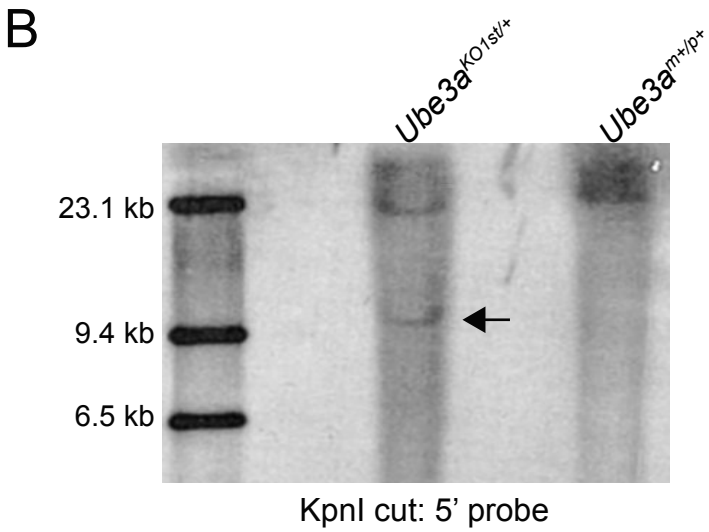

KpnI cut: 5' probe

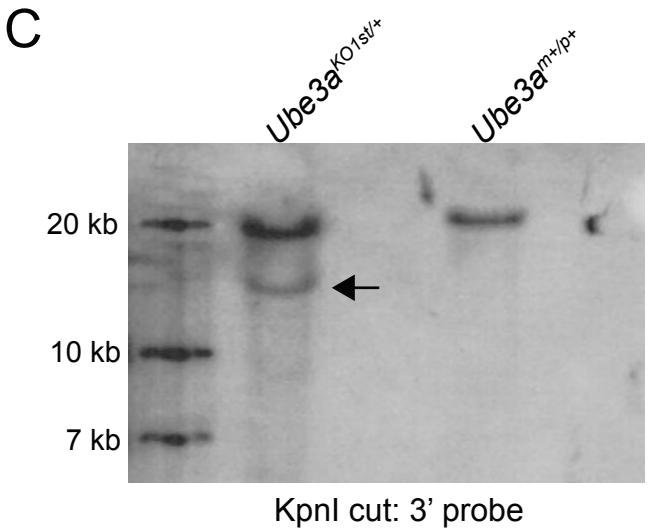

KpnI cut: 3' probe

Figure S2

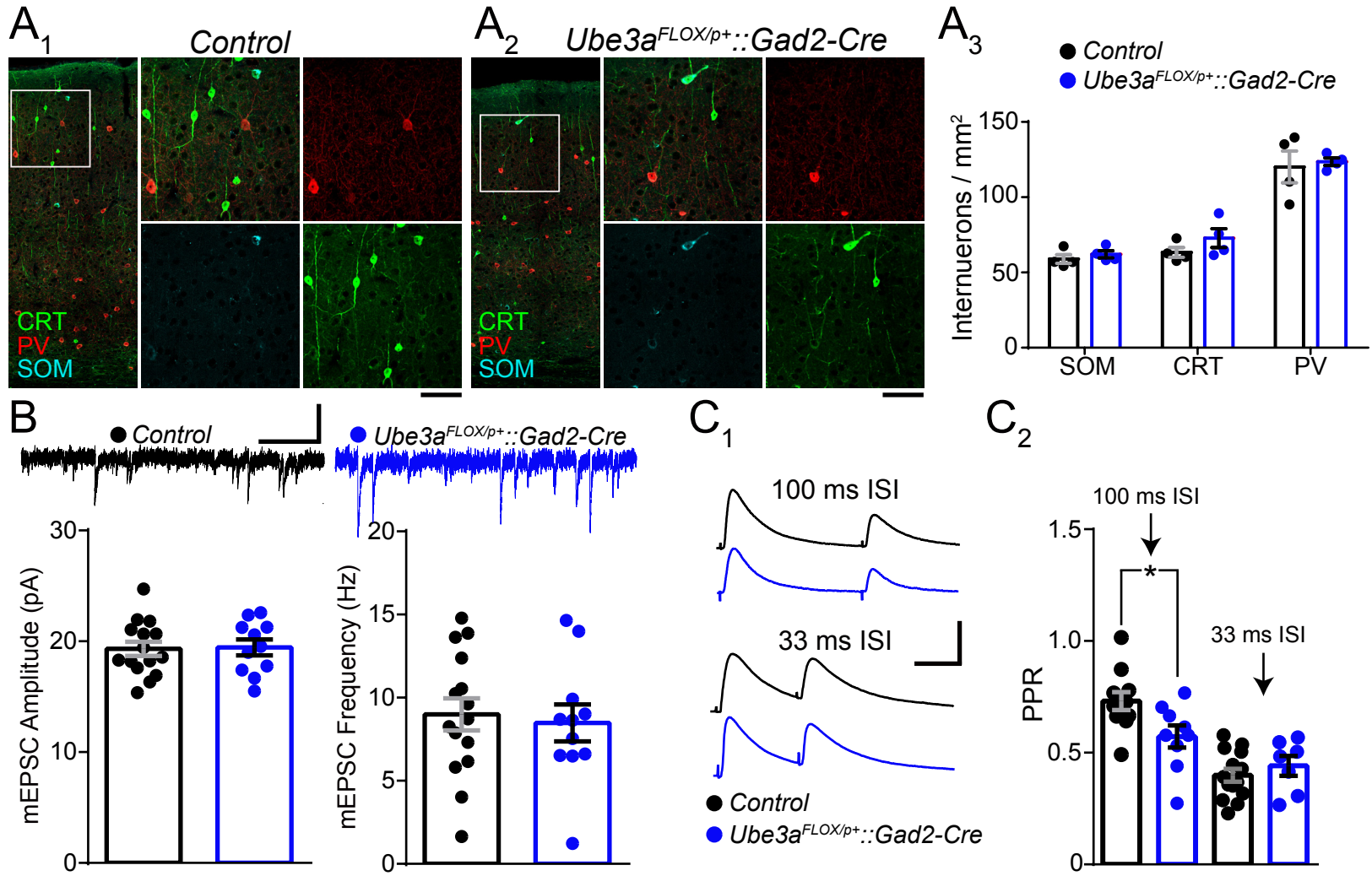
A1
Control
A2
Ube3aFLOX/p+::Gad2-Cre
A3
Control
Ube3aFLOX/p+::Gad2-Cre
CRT
PV
SOM
Interneurons / mm2
150
100
50
0
SOM
CRT
PV
B
Control
Ube3aFLOX/p+::Gad2-Cre
mEPSC Amplitude (pA)
30
20
10
0
mEPSC Frequency (Hz)
20
15
10
5
0
C1
100 ms ISI
33 ms ISI
Control
Ube3aFLOX/p+::Gad2-Cre
C2
100 ms ISI
33 ms ISI
PPR
1.5
1.0
0.5
0
*

Figure S3

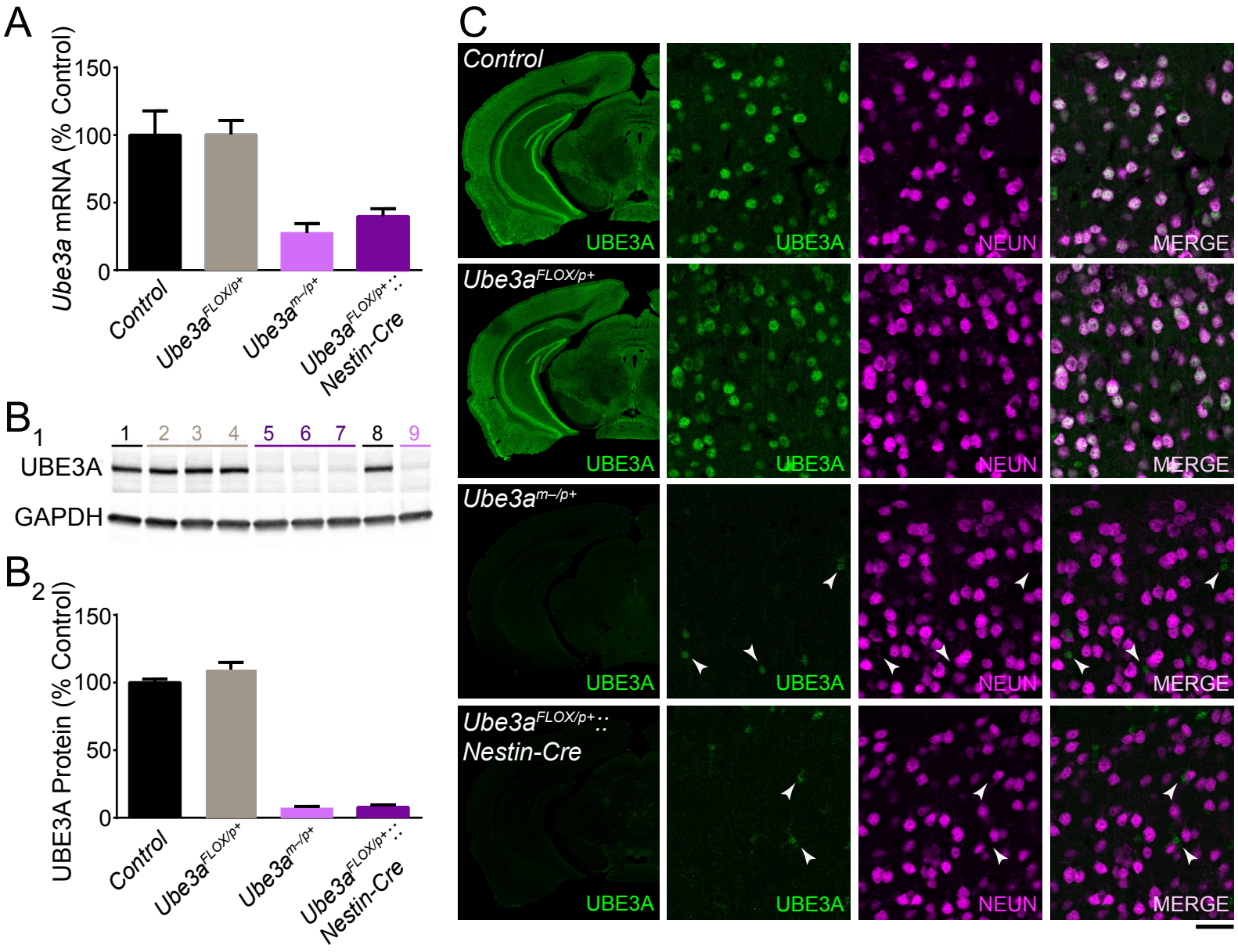
A
Ube3a mRNA (% Control)
150
100
50
0
Control
Ube3a^FLOX/p+
Ube3a^m−/p+
Ube3a^FLOX/p+::Nestin-Cre
B1
1 2 3 4 5 6 7 8 9
UBE3A
GAPDH
B2
UBE3A Protein (% Control)
150
100
50
0
Control
Ube3a^FLOX/p+
Ube3a^m−/p+
Ube3a^FLOX/p+::Nestin-Cre
C
Control
Ube3a^FLOX/p+
Ube3a^m−/p+
Ube3a^FLOX/p+::Nestin-Cre
UBE3A
NEUN
MERGE

Figure S4

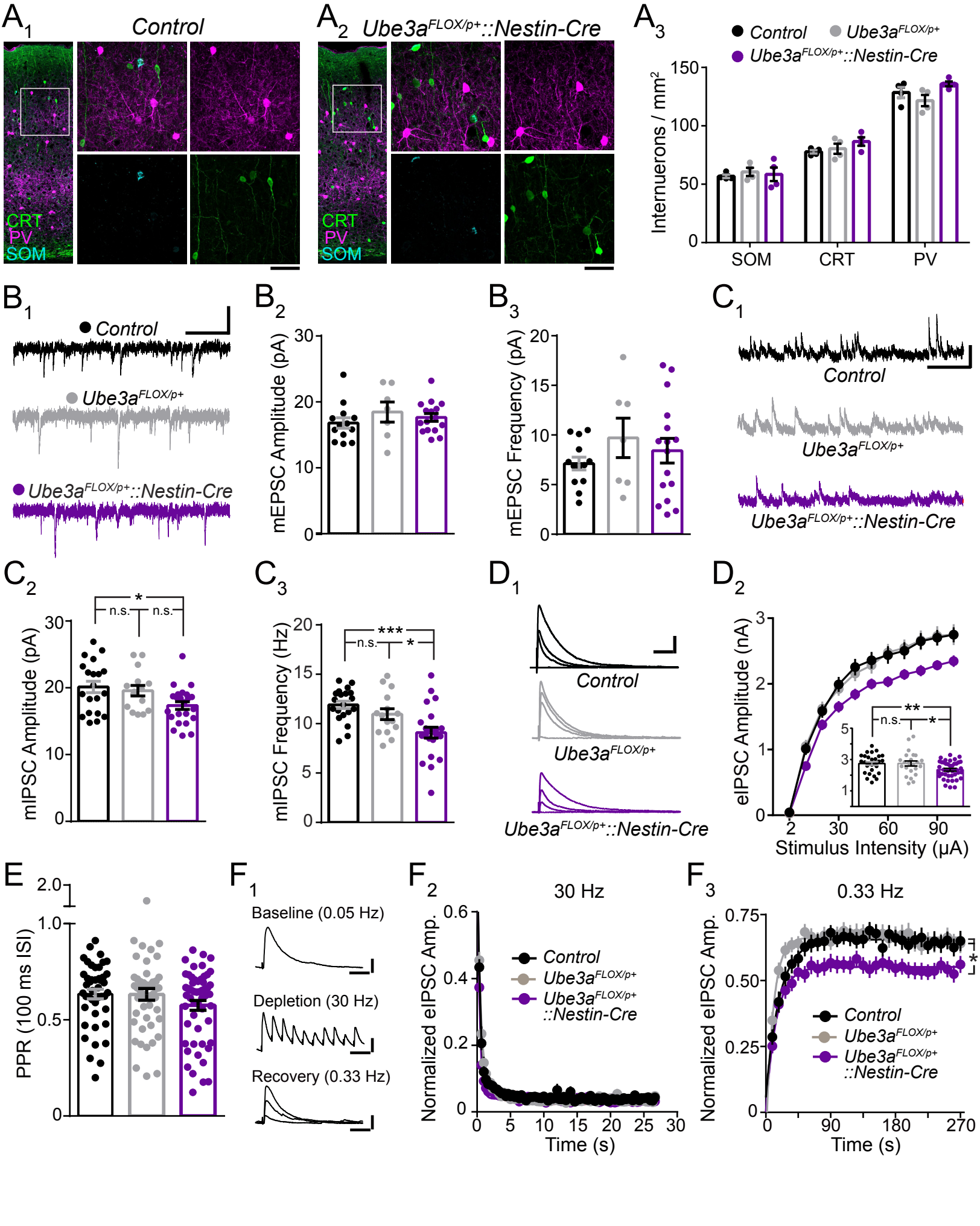
A1
Control
A2
Ube3a^FLOX/p+::Nestin-Cre
CRT
PV
SOM
A3
Control
Ube3a^FLOX/p+
Ube3a^FLOX/p+::Nestin-Cre
Internuerons / mm2
150
100
50
0
SOM
CRT
PV
B1
Control
Ube3a^FLOX/p+
Ube3a^FLOX/p+::Nestin-Cre
B2
mEPSC Amplitude (pA)
30
20
10
0
B3
mEPSC Frequency (pA)
20
15
10
5
0
C1
Control
Ube3a^FLOX/p+
Ube3a^FLOX/p+::Nestin-Cre
C2
mIPSC Amplitude (pA)
*
n.s.
n.s.
30
20
10
0
C3
mIPSC Frequency (Hz)
***
n.s.
*
20
15
10
5
0
D1
Control
Ube3a^FLOX/p+
Ube3a^FLOX/p+::Nestin-Cre
D2
eIPSC Amplitude (nA)
3
2
1
0
**
n.s.
*
5
3
1
2
30
60
90
Stimulus Intensity (μA)
E
PPR (100 ms ISI)
2.0
1.0
0.5
0
F1
Baseline (0.05 Hz)
Depletion (30 Hz)
Recovery (0.33 Hz)
F2
30 Hz
Normalized eIPSC Amp.
0.6
0.4
0.2
0
Control
Ube3a^FLOX/p+
Ube3a^FLOX/p+
::Nestin-Cre
0
5
10
15
20
25
30
Time (s)
F3
0.33 Hz
Normalized eIPSC Amp.
0.75
0.50
0.25
0
*
Control
Ube3a^FLOX/p+
Ube3a^FLOX/p+
::Nestin-Cre
0
90
180
270
Time (s)

Figure S5

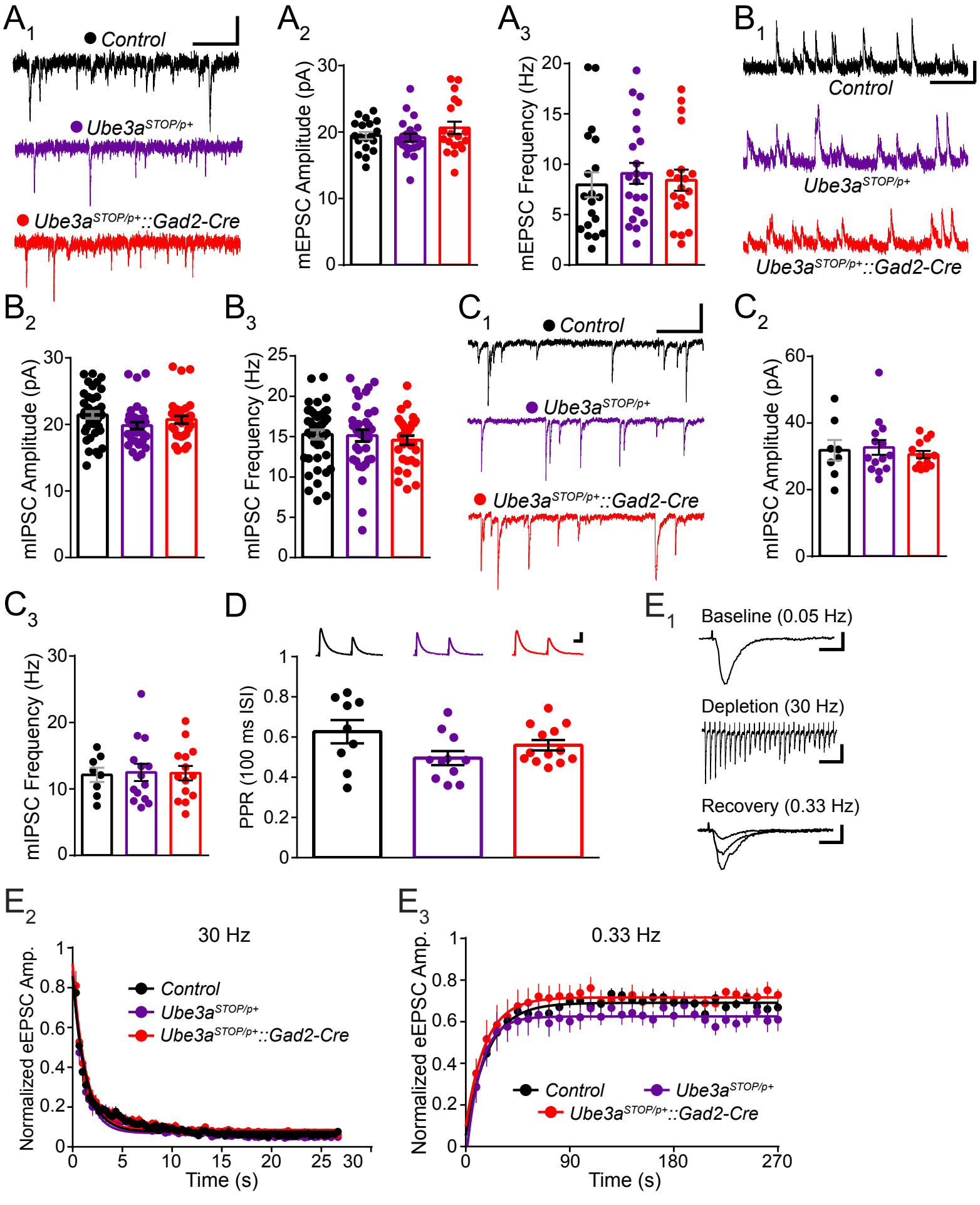
A1
Control
Ube3aSTOP/p+
Ube3aSTOP/p+::Gad2-Cre
A2
mEPSC Amplitude (pA)
A3
mEPSC Frequency (Hz)
B1
Control
Ube3aSTOP/p+
Ube3aSTOP/p+::Gad2-Cre
B2
mIPSC Amplitude (pA)
B3
mIPSC Frequency (Hz)
C1
Control
Ube3aSTOP/p+
Ube3aSTOP/p+::Gad2-Cre
C2
mIPSC Amplitude (pA)
C3
mIPSC Frequency (Hz)
D
PPR (100 ms ISI)
E1
Baseline (0.05 Hz)
Depletion (30 Hz)
Recovery (0.33 Hz)
E2
30 Hz
Normalized eEPSC Amp.
Control
Ube3aSTOP/p+
Ube3aSTOP/p+::Gad2-Cre
Time (s)
E3
0.33 Hz
Normalized eEPSC Amp.
Control
Ube3aSTOP/p+
Ube3aSTOP/p+::Gad2-Cre
Time (s)

Figure S6

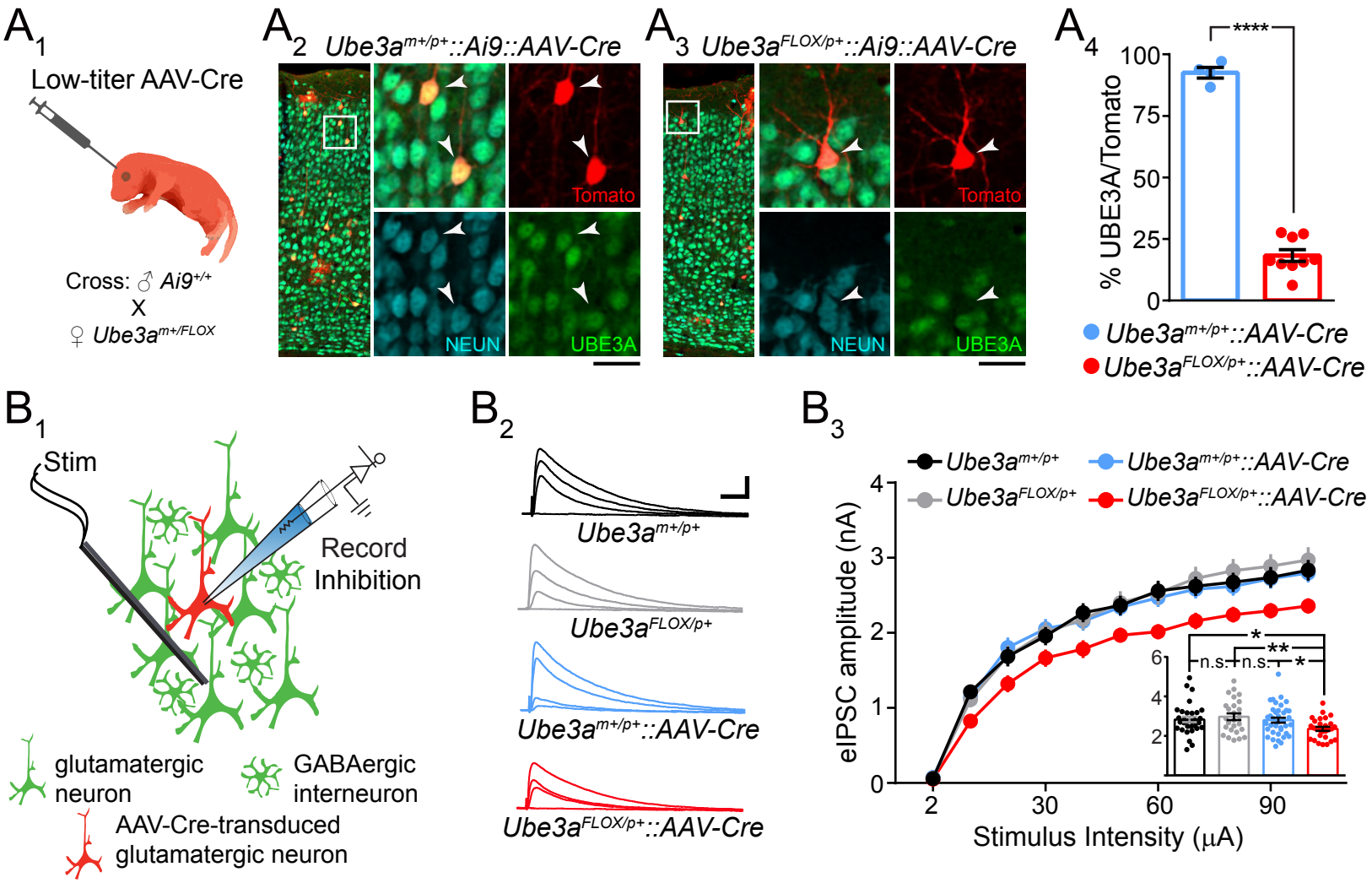
A1
Low-titer AAV-Cre
Cross: ♂ Ai9+/+
X
♀ Ube3am+/FLOX
A2 Ube3am+/p+::Ai9::AAV-Cre
Tomato
NEUN
UBE3A
A3 Ube3aFLOX/p+::Ai9::AAV-Cre
Tomato
NEUN
UBE3A
A4
****
% UBE3A/Tomato
100
75
50
25
0
Ube3am+/p+::AAV-Cre
Ube3aFLOX/p+::AAV-Cre
B1
Stim
Record
Inhibition
glutamatergic neuron
GABAergic interneuron
AAV-Cre-transduced glutamatergic neuron
B2
Ube3am+/p+
Ube3aFLOX/p+
Ube3am+/p+::AAV-Cre
Ube3aFLOX/p+::AAV-Cre
B3
Ube3am+/p+
Ube3am+/p+::AAV-Cre
Ube3aFLOX/p+
Ube3aFLOX/p+::AAV-Cre
eIPSC amplitude (nA)
Stimulus Intensity (μA)
n.s.
n.s.
*
**
*

Figure S7

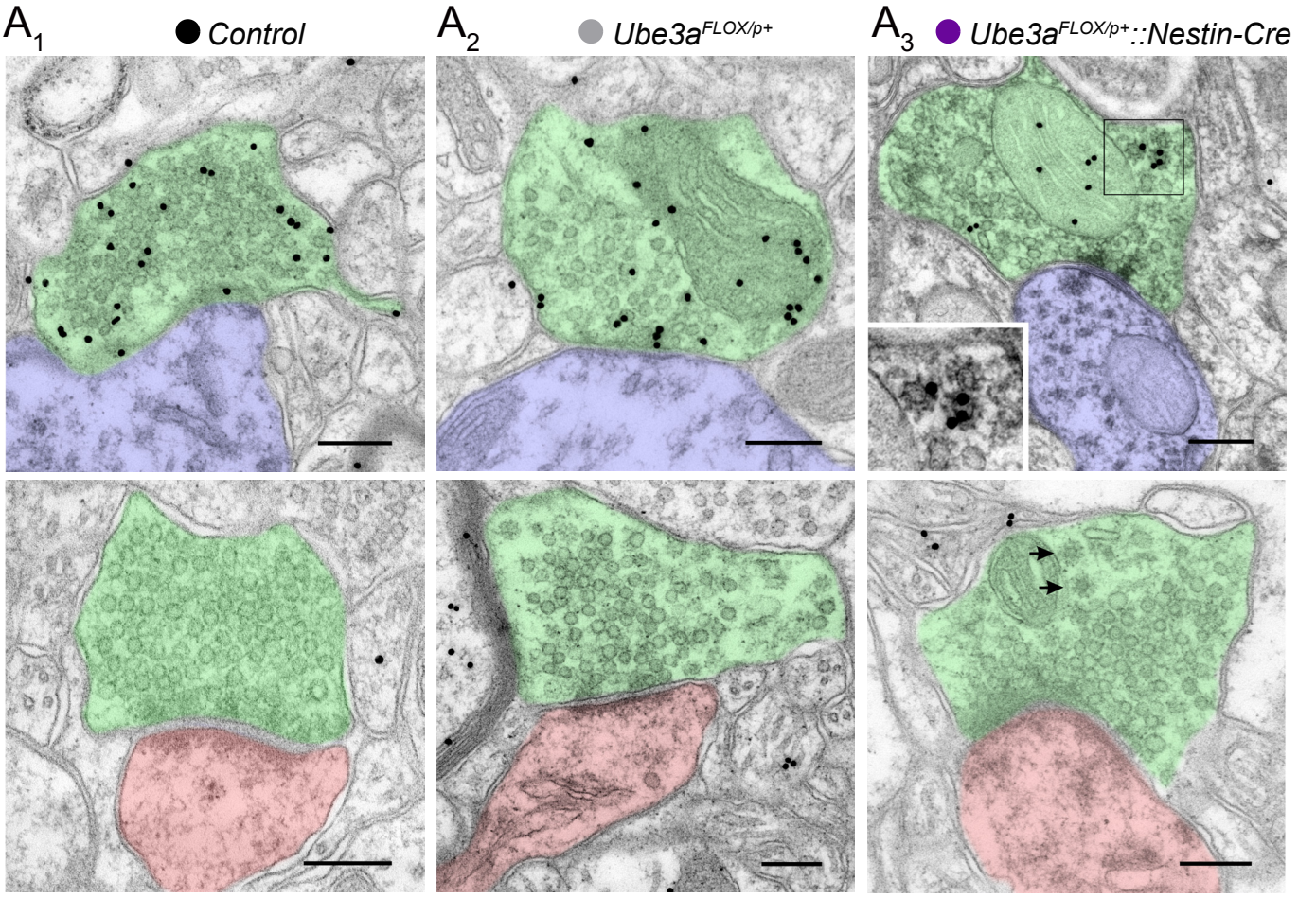
A1
Control
A2
Ube3aFLOX/p+
A3
Ube3aFLOX/p+::Nestin-Cre

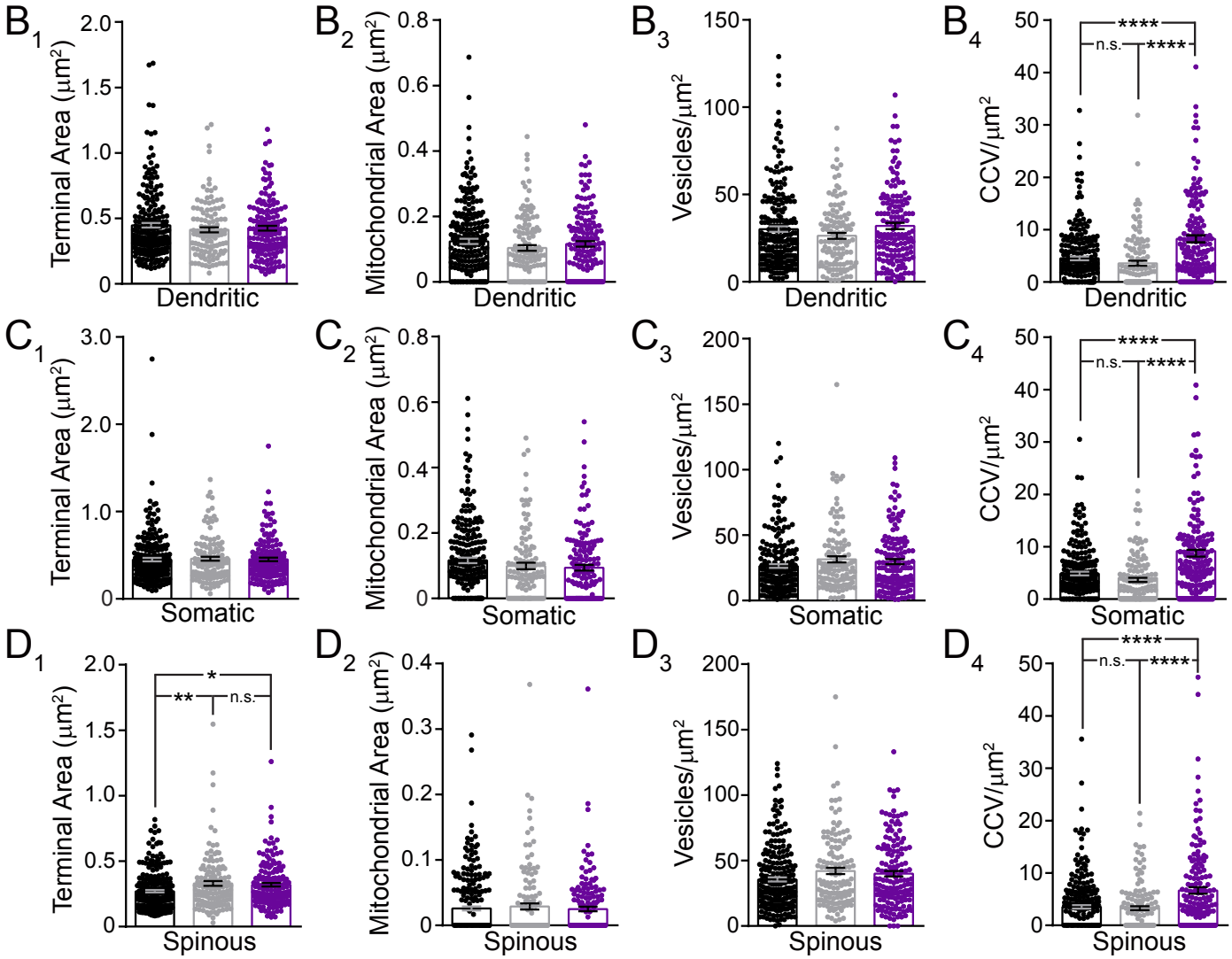
B1
Terminal Area (µm2)
Dendritic
B2
Mitochondrial Area (µm2)
Dendritic
B3
Vesicles/µm2
Dendritic
B4
CCV/µm2
****
n.s.
****
Dendritic
C1
Terminal Area (µm2)
Somatic
C2
Mitochondrial Area (µm2)
Somatic
C3
Vesicles/µm2
Somatic
C4
CCV/µm2
****
n.s.
****
Somatic
D1
Terminal Area (µm2)
*
**
n.s.
Spinous
D2
Mitochondrial Area (µm2)
Spinous
D3
Vesicles/µm2
Spinous
D4
CCV/µm2
****
n.s.
****
Spinous

Figure S8

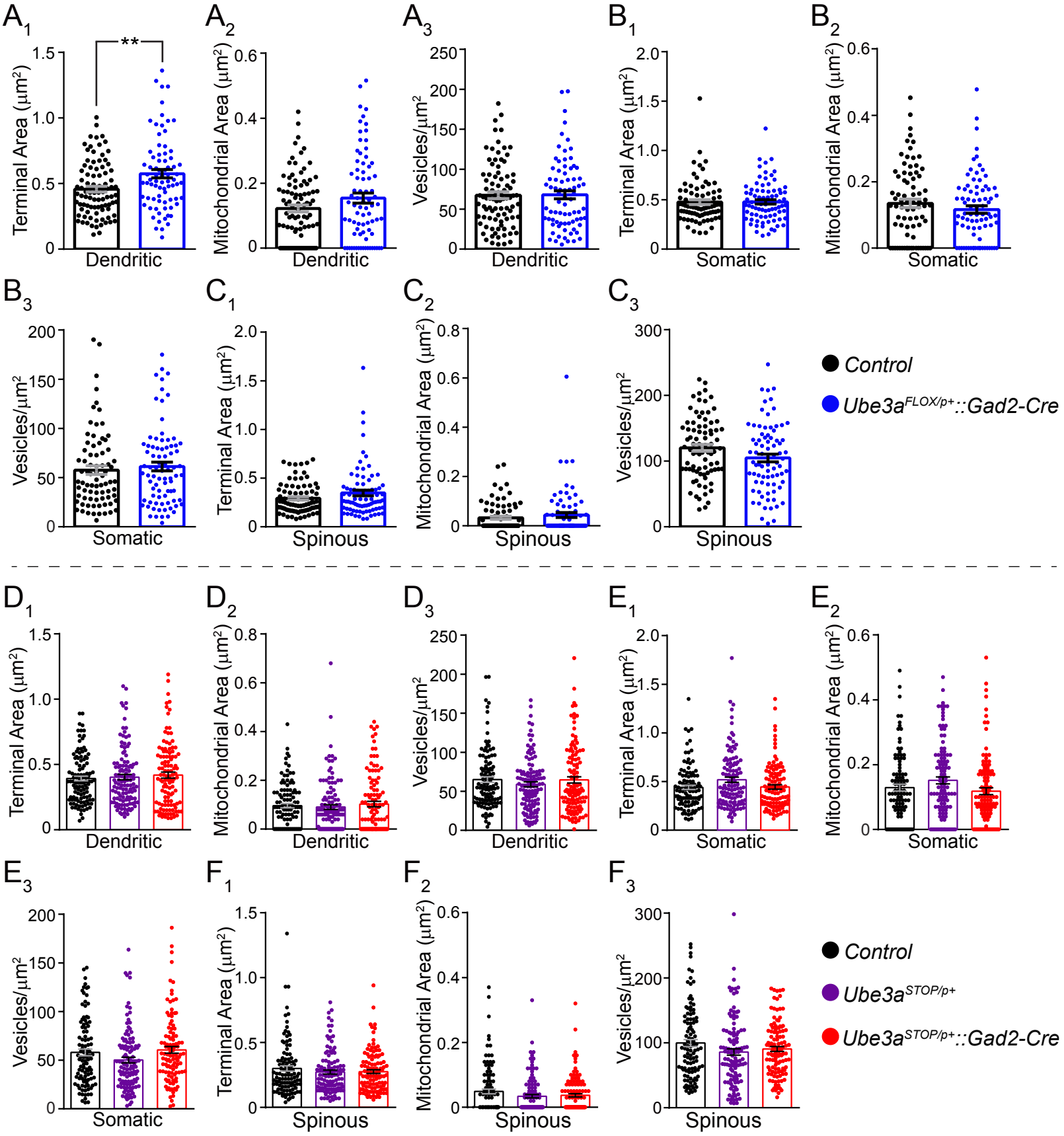
A1
A2
A3
B1
B2
B3
C1
C2
C3
D1
D2
D3
E1
E2
E3
F1
F2
F3
**
Terminal Area (µm²)
Mitochondrial Area (µm²)
Vesicles/µm²
Dendritic
Somatic
Spinous
Control
Ube3aFLOX/p+::Gad2-Cre
Ube3aSTOP/p+
Ube3aSTOP/p+::Gad2-Cre

SUPPLEMENTAL FIGURE LEGENDS

Figure S1 (related to Figures 1, 3-7). Validation of *Ube3a^{KO1st}*-targeted embryonic stem cells.

(**A**) Schematic of strategy to generate C57BL/6 mice carrying the *Ube3a^{FLOX}* allele, as previously described (Berrios et al., 2016). (**B**) Southern blotting of genomic DNA from wild type (*Ube3a$^{m+/p+}$*) and *Ube3a^{KO1st}*-targeted embryonic stem cells probe specific to 5' end of the targeted *Ube3a* genomic region. (**C**) Southern blotting of the same samples using a probe specific to the 3' end of the targeted *Ube3a* genomic region. Arrows indicate KpnI-digested fragments specifically resulting from the *Ube3a^{KO1st}* allele.

Figure S2 (related to Figures 1 and 3). Analyses of interneuron density, miniature EPSCs, and evoked IPSC paired-pulse ratios following GABAergic deletion of *Ube3a*.

(**A**) Immunostaining of interneuron subtype-specific markers calretinin (CRT), parvalbumin (PV), and somatostatin (SOM) in ~P80 primary visual cortex of *Control* (A_1) and *Ube3a$^{FLOX/p+}$::Gad2-Cre* (A_2) mice. (A_3) Quantification of SOM-, CRT-, and PV-positive interneuron density (*Control* n = 4 mice; *Ube3a$^{FLOX/p+}$::Gad2-Cre* n = 4 mice). (**B**) Sample recordings and quantification of mEPSC amplitude and frequency from pyramidal neurons in ~P80 L2/3 visual cortex from *Control* (n = 15 cells) and *Ube3a$^{FLOX/p+}$::Gad2-Cre* (n = 11 cells) mice. (**C**) Sample recordings (C_1) and quantification (C_2) of eIPSC paired pulse ratios in ~P80 *Control* and *Ube3a$^{FLOX/p+}$::Gad2-Cre* mice using both 100 ms (*Control* n = 11 cells; *Ube3a$^{FLOX/p+}$::Gad2-Cre* n = 9 cells) and 33 ms (*Control* n = 14 cells; *Ube3a$^{FLOX/p+}$::Gad2-Cre* n = 7 cells) interstimulus intervals (ISI). Scale bars: 100 μm or 50 μm for zoom-ins (A); 20 pA, 200 ms (B); 200 pA, 20 ms (C_1, 100 ms ISI); 200 pA, 12 ms (C_1, 33 ms ISI). Data represent mean ± SEM. *p≤0.05.

Figure S3 (related to Figures 1, 3-7). Cre-mediated recombination of the maternally inherited *Ube3a^{FLOX}* allele nullifies neuronal *Ube3a* expression.

(**A**) qRT-PCR analysis of *Ube3a* expression in ~P60 neocortex (*Control* n = 6 mice; *Ube3a$^{FLOX/p+}$* n = 4 mice; *Ube3a$^{m-/p+}$* n = 3 mice; *Ube3a$^{FLOX/p+}$::Nestin-Cre* n = 4 mice). (**B**) Representative Western blots (B_1) for UBE3A and GAPDH loading control protein prepared from ~P60 neocortical lysates. Lanes: *Control* = 1 and 8; *Ube3a$^{FLOX/p+}$* = 2-4; *Ube3a$^{FLOX/p+}$::Nestin-Cre* = 5-7; *Ube3a$^{m-/p+}$* = 9. (B_2) Quantification of Western blotting (*Control* n = 3 mice; *Ube3a$^{FLOX/p+}$* n = 5 mice; *Ube3a$^{m-/p+}$* n = 2 mice; *Ube3a$^{FLOX/p+}$::Nestin-Cre* n = 6 mice). (**C**) UBE3A immunostaining at ~P80 in posterior coronal hemisections (far left column) and in L2/3 of primary visual cortex in conjunction with staining for the neuronal marker NEUN. Arrowheads indicate UBE3A staining in NEUN-negative glia (scale bar = 1.1 mm for hemisections and 35 μm for L2/3 visual cortex. Data represent mean ± SEM.

Figure S4 (related to Figures 1 and 3). Nervous system-specific deletion of maternal *Ube3a* results in inhibitory synaptic defects onto L2/3 pyramidal neurons.

(**A**) Immunostaining of interneuron subtype-specific markers calretinin (CRT), parvalbumin (PV), and somatostatin (SOM) in ~P80 primary visual cortex of *Control* (A_1) and *Ube3a$^{FLOX/p+}$::Nestin-Cre* (A_2) mice. Scale bar = 100 μm or 40 μm for zoom-ins. (A_3) Quantification of SOM-, CRT-, and PV-positive interneuron density (*Control* n = 4 mice; *Ube3a$^{FLOX/p+}$* n = 4 mice; *Ube3a$^{FLOX/p+}$::Nestin-Cre* n = 4 mice). (**B**) Sample recordings (B_1, scale bar = 20 pA, 200 ms) and quantification of mEPSC amplitude (B_2) and frequency (B_3) from pyramidal neurons in ~P80 L2/3 visual cortex from *Control* (n = 13 cells), *Ube3a$^{FLOX/p+}$* (n = 7 cells), and *Ube3a$^{FLOX/p+}$::Nestin-Cre* (n = 16 cells). (**C**) Sample mIPSC recordings (C_1) from pyramidal neurons in ~P80 L2/3 visual cortex (scale bar = 20 pA, 200 ms). Quantification of mIPSC amplitude (C_2) and frequency (C_3) (*Control* n = 20 cells; *Ube3a$^{FLOX/p+}$* n = 15 cells; *Ube3a$^{FLOX/p+}$::Nestin-Cre* n = 23 cells). (**D**) Sample recordings of eIPSCs (D_1) at stimulation intensities of 2, 10, 30, and 100 μA (scale bar = 900 pA, 50 ms). (D_2) Quantification of

eIPSCs at ~P80. Inset depicts response amplitudes to 100 μA stimulation (*Control* n = 28 cells; *Ube3a*$^{FLOX/p+}$ n = 23 cells; *Ube3a*$^{FLOX/p+}$*::Nestin-Cre* n = 40 cells). (**E**) Quantification of eIPSCs in paired-pulse experiments (*Control* n = 44 cells; *Ube3a*$^{FLOX/p+}$ n = 51 cells; *Ube3a*$^{FLOX/p+}$*::Nestin-Cre* n = 54 cells). (**F**) Sample recordings (F_1) depicting each phase of an inhibitory synaptic depletion and recovery experiment performed in ~P80 mice (scale bars: baseline = 200 pA, 20 ms; depletion = 200 pA, 70 ms; recovery = 200 pA, 20 ms). (F_2) Average depletion phase showing eIPSC amplitude normalized to baseline during 800 stimuli at 30 Hz. Each point (80 plotted per genotype) represents the average of 10 consecutive responses that were collapsed and averaged per cell. (F_3) Average recovery phase showing eIPSC amplitude normalized to baseline during 90 stimuli at 0.33 Hz. Each point (30 plotted per genotype) represents the average of 3 consecutive responses that were collapsed and averaged per cell. Average depletion and recovery responses for each genotype were fit with a monophasic exponential (*Control* n = 43 cells; *Ube3a*$^{FLOX/p+}$ n = 51 cells; *Ube3a*$^{FLOX/p+}$*::Nestin-Cre* n = 53 cells). Data represent mean ± SEM. *p≤0.05, ***p≤0.001.

Figure S5 (related to Figure 2). Analyses of miniature EPSCs, miniature IPSCs, evoked IPSC paired-pulse ratios, and excitatory synaptic depletion following GABAergic reinstatement of *Ube3a*.

(**A**) Sample recordings (A_1, scale bar = 20 pA, 200 ms) and quantification of mEPSC amplitude (A_2) and frequency (A_3) from pyramidal neurons in ~P80 L2/3 visual cortex from *Control* (n = 19 cells), *Ube3a*$^{STOP/p+}$ (n = 22 cells), and *Ube3a*$^{STOP/p+}$*::Gad2-Cre* (n = 19 cells). (**B**) Sample mIPSC recordings, using a standard internal solution (B_1), from pyramidal neurons in ~P80 L2/3 visual cortex (scale bar = 20 pA, 200 ms), with quantification of mIPSC amplitude (B_2) and frequency (B_3) (*Control* n = 43 cells; *Ube3a*$^{STOP/p+}$ n = 34 cells; *Ube3a*$^{STOP/p+}$*::Gad2-Cre* n = 30 cells). (**C**) Sample mIPSC recordings, using a high-chloride internal solution (C_1), from pyramidal neurons in ~P80 L2/3 visual cortex (scale bar = 50 pA, 200 ms), with quantification of mIPSC amplitude (C_2) and mIPSC

frequency (C_3) (*Control* n = 8 cells; *Ube3a*$^{STOP/p+}$ n = 14 cells; *Ube3a*$^{STOP/p+}$*::Gad2-Cre* n = 14 cells). (**D**) Sample recordings (scale bar = 200 pA, 25 ms) and quantification of eIPSCs in paired-pulse experiments (*Control* n = 9 cells; *Ube3*$^{STOP/p+}$ n = 11 cells; *Ube3a*$^{STOP/p+}$*::Gad2-Cre* n = 13 cells). (**E**) Sample recordings (E_1) depicting each phase of an excitatory synaptic depletion and recovery experiment performed in ~P80 mice (scale bars: baseline = 60 pA, 8 ms; depletion = 60 pA, 160 ms; recovery = 60 pA, 8 ms). (E_2) Average depletion phase showing eEPSC amplitude normalized to baseline during 800 stimuli at 30 Hz. Each point (80 plotted per genotype) represents the average of 10 consecutive responses that were collapsed and averaged per cell. (E_3) Average recovery phase showing eEPSC amplitude normalized to baseline during 90 stimuli at 0.33 Hz. Each point (30 plotted per genotype) represents the average of 3 consecutive responses that were collapsed and averaged per cell. Average depletion and recovery responses for each genotype were fit with a monophasic exponential (*Control* n = 13 cells; *Ube3a*$^{STOP/p+}$ n = 11 cells; *Ube3a*$^{STOP/p+}$*::Gad2-Cre* n = 11 cells). Data represent mean ± SEM.

Figure S6 (related to Figure 3). Decreased evoked IPSC amplitude following cell-autonomous glutamatergic *Ube3a* loss.

(**A**) Intracerebroventricular injection strategy (A_1) used to achieve mosaic AAV-Cre transduction of L2/3 pyramidal neurons in *Ube3a*$^{FLOX/p+}$ and *Ube3a*$^{m+/p+}$ control littermates expressing the *Ai9* Cre-dependent tdTomato reporter allele. Immunostaining of UBE3A and the neuronal marker NEUN in P12 *Ube3a*$^{m+/p+}$*::Ai9* (A_2) and *Ube3a*$^{FLOX/p+}$*::Ai9* (A_3) mice neonatally injected with low-titer AAV-Cre. Arrowheads point to AAV-Cre-transduced, tdTomato-positive L2/3 pyramidal neurons (scale bar = 125 μm or 30 μm for zoom-ins). (A_4) Quantification at P12 of the percentage of tdTomato and UBE3A co-stained neurons per image, each of which depict an 800 μm-wide strip of cortex (*Ube3a*$^{m+/p+}$ n = 5 images; *Ube3a*$^{FLOX/p+}$ n = 10 images). (**B**) Schematic for recording eIPSCs (B_1) from L2/3 pyramidal neurons in AAV-Cre-transduced primary visual cortex. (B_2) Sample recordings of eIPSCs at

stimulation intensities of 2, 10, 30, and 100 μA (scale bar = 1 nA, 40 ms). (B_3) Quantification of eIPSCs recorded at ~P80. Inset depicts response amplitudes to 100 μA stimulation (*Ube3a*$^{m+/p+}$ n = 32 cells; *Ube3a*$^{FLOX/p+}$ n = 26 cells; *Ube3a*$^{m+/p+}$*::AAV-Cre* n = 38 cells; *Ube3a*$^{FLOX/p+}$*::AAV-Cre* n = 28 cells). Data represent mean ± SEM. *p≤0.05, **p≤0.01, ****p≤0.0001.

Figure S7 (related to Figure 7). Nervous system-specific deletion of *Ube3a* causes CCV accumulation at both glutamatergic and GABAergic neocortical synapses.

(**A**) Electron micrographs of dendritic inhibitory synapses stained for GABA (top row) and glutamatergic spinous synapses (bottom row) in *Control* (A_1), *Ube3a*$^{FLOX/p+}$ (A_2), and *Ube3a*$^{FLOX/p+}$*::Nestin-Cre* (A_3) mice at ~P80. Green denotes GABAergic axon terminal, blue denotes dendrite, red denotes dendritic spine, inset or arrows highlight clathrin coated vesicles (CCVs) (scale bar = 200 nm). (**B**) Average values at dendritic inhibitory synapses for axon terminal area (B_1), terminal mitochondrial area (B_2), synaptic vesicles per μm^2 (B_3), and CCVs per μm^2 (B_4) (*Control* n = 216 synapses from 6 mice; *Ube3a*$^{FLOX/p+}$ n = 117 synapses from 3 mice; *Ube3a*$^{FLOX/p+}$*::Nestin-Cre* n = 151 synapses from 4 mice). (**C**) Average values at somatic inhibitory synapses for axon terminal area (C_1), terminal mitochondrial area (C_2), synaptic vesicles per μm^2 (C_3), and CCVs per μm^2 (C_4) (*Control* n = 213 synapses from 6 mice; *Ube3a*$^{FLOX/p+}$ n = 123 synapses from 3 mice; *Ube3a*$^{FLOX/p+}$*::Nestin-Cre* n = 149 synapses from 4 mice). (**D**) Average values at glutamatergic (spinous) synapses for axon terminal area (D_1), terminal mitochondrial area (D_2), synaptic vesicles per μm^2 (D_3), and CCVs per μm^2 (D_4) (*Control* n = 241 synapses from 6 mice; *Ube3a*$^{FLOX/p+}$ n = 132 synapses from 3 mice; *Ube3a*$^{FLOX/p+}$*::Nestin-Cre* n = 156 synapses from 4 mice). Data represent mean ± SEM. *p≤0.05, **p≤0.01, ****p≤0.0001.

Figure S8 (related to Figure 7). Ultrastructural analyses of presynaptic terminal size, mitochondrial representation, and synaptic vesicle density following GABAergic *Ube3a* deletion and reinstatement.

(**A-C**) Average values from ~P80 *Control* and *Ube3a*$^{FLOX/p+}$*::Gad2-Cre* mice at L2/3 GABAergic synapses onto dendrites (A_1-A_3, *Control* n = 89 synapses from 3 mice; *Ube3a*$^{FLOX/p+}$*::Gad2-Cre* n = 77 synapses from 3 mice), L2/3 GABAergic synapses onto somata (B_1-B_3, *Control* n = 78 synapses from 3 mice; *Ube3a*$^{FLOX/p+}$*::Gad2-Cre* n = 81 synapses from 3 mice), and L2/3 glutamatergic spinous synapses (C_1-C_3, *Control* n = 82 synapses from 3 mice; *Ube3a*$^{FLOX/p+}$*::Gad2-Cre* n = 80 synapses from 3 mice). (**D-F)** Average values from ~P80 *Control*, *Ube3a*$^{STOP/p+}$, and *Ube3a*$^{STOP/p+}$*::Gad2-Cre* mice at L2/3 GABAergic synapses onto dendrites (D_1-D_3, *Control* n = 110 synapses from 3 mice; *Ube3a*$^{STOP/p+}$ n = 119 synapses from 3 mice; *Ube3a*$^{STOP/p+}$*::Gad2-Cre* n = 115 synapses from 3 mice), L2/3 GABAergic synapses onto somata (E_1-E_3, *Control* n = 103 synapses from 3 mice; *Ube3a*$^{STOP/p+}$ n = 114 synapses from 3 mice; *Ube3a*$^{STOP/p+}$*::Gad2-Cre* n = 110 synapses from 3 mice), and L2/3 glutamatergic spinous synapses (F_1-F_3, *Control* n = 108 synapses from 3 mice; *Ube3a*$^{STOP/p+}$ n = 113 synapses from 3 mice; *Ube3a*$^{STOP/p+}$*::Gad2-Cre* n = 113 synapses from 3 mice). Data represent mean ± SEM. **p≤0.01.

Table S1 (related to Figures 1, 3, S4, and S5). Quantification of membrane properties from mIPSC experiments

Figure S4C (mIPSCs)				
Genotype:	*Control*	*Ube3a*$^{FLOX/p+}$	*Ube3a*$^{FLOX/p+}$*::Nestin-Cre*	p-value
n =	20	15	23	
*Cm (pF)	169.9 ± 7.5	158.86 ± 8.65	156.35 ± 5.47	0.34
Rs (MΩ)	14.7 ± 0.84	14.62 ± 0.6	13.99 ± 0.69	0.74
Rm (MΩ)	213.2 ± 15.8	236.26 ± 16.1	241.26 ± 16.12	0.41
*Tau (ms)	1.9 ± 0.13	1.8 ± 0.14	1.8 ± 0.1	0.86
Figure 1C (mIPSCs)				
Genotype:	*Control*	*Ube3a*$^{FLOX/p+}$*::Gad2-Cre*	p-value	
n =	11	17		
*Cm (pF)	167.45 ± 8.83	162.53 ± 6.79	0.66	
Rs (MΩ)	13.98 ± 1.31	13.72 ± 0.86	0.87	
Rm (MΩ)	218.92 ± 26.12	223.87 ± 5.91	0.82	
*Tau (ms)	1.59 ± 0.17	1.62 ± 0.1	0.64	
Figure 3F (mIPSCs)				
Genotype:	*Control*	*Ube3a*$^{FLOX/p+}$*::NEX-Cre*	p-value	
n =	15	12		
*Cm (pF)	152.07 ± 5.66	157.75 ± 9.73	0.62	
Rs (MΩ)	15.52 ± 1.12	16.08 ± 1.49	0.77	
Rm (MΩ)	188.13 ± 8.57	195.5 ± 14.83	0.67	
*Tau (ms)	2.17 ± 0.16	2.2 ± 0.19	0.90	
Figure S5B (mIPSCs)				
Genotype:	*Control*	*Ube3a*$^{STOP/p+}$	*Ube3a*$^{STOP/p+}$*::Gad2-Cre*	p-value
n =	43	34	30	
*Cm (pF)	174.11 ± 4.39	165.9 ± 4.95	173.96 ± 7.0	0.47
Rs (MΩ)	11.13 ± 0.54	11.09 ± 0.61	10.91 ± 0.64	0.97
Rm (MΩ)	183.13 ± 8.06	186.45 ± 9.82	189.51 ± 10.15	0.89
*Tau (ms)	1.78 ± 0.08	1.71 ± 0.1	1.74 ± 0.08	0.83

Cm, capacitance; Rs, series resistance; Rm, membrane resistance; Tau, membrane time constant. *Values estimated using membrane test feature in pClamp 10.

SUPPLEMENTAL EXPERIMENTAL PROCEDURES

Animals

We generated *Ube3a*^{FLOX} mice in the UNC Animal Models Core facility. Briefly, we electroporated C57BL/6 mouse embryonic stem (ES) cells with an AsiSI-linearized *Ube3a*^{KO1st} targeting construct, which was generated by the trans-NIH Knockout Mouse Project (KOMP) and obtained from the KOMP repository (www.komp.org). We then analyzed DNA from neomycin-resistant ES cell colonies by Southern blot hybridization using both 5'- and 3'-flanking probes to confirm clones which had incorporated the *Ube3a*^{KO1st} allele via homologous recombination. To produce *Ube3a*^{KO1st}-targeted chimeric mice, we microinjected *Ube3a*^{KO1st}-targeted ES cells into C57BL/6-albino blastocysts. We then crossed germline chimeric males (determined by transmission of coat color in parallel breeding) to C57BL/6 female homozygous *Rosa26-FLPe* mice (RRID:IMSR_JAX:009086) in order to excise the *FRT*-flanked lacZ gene trap from the *Ube3a*^{KO1st} allele and thereby produce the conditional *Ube3a* knockout allele (i.e., *Ube3a*^{FLOX}). We bred the *FLPe* allele out of the *Ube3a*^{FLOX} line and maintained *Ube3a*$^{m+/FLOX}$ female breeders on a congenic C57BL/6 background, except for *in vivo* LFP and audiogenic seizure experiments, in which case *Ube3a*$^{m+/FLOX}$ female breeders were backcrossed at least 5 times onto the129S2/SvPasCrl background. We genotyped *Ube3a*^{FLOX} mice using the following polymerase chain reaction (PCR) primers: *Ube3a*^{FLOX} F (5′- AAAATTGGGTATGCGAGCTG -3′) and *Ube3a*^{FLOX} R (5′- GGGGTCTAAGGGCCTATGAA -3′).

The laboratory of Ype Elgersma originally generated *Ube3a*^{STOP} mice on a congenic 129S2/SvPasCrl background (Silva-Santos et al., 2015). We maintained *Ube3a*$^{m+/STOP}$ females on the congenic 129S2/SvPasCrl background to support breeding for *in vivo* LFP recordings and audiogenic seizure experiments, but used *Ube3a*$^{m+/STOP}$ females backcrossed 2-4 generations onto the C57BL/6J background for breeding to supply whole-cell electrophysiology and electron microscopy experiments.

Most experiments required the mating of female mice with paternal inheritance of a conditional *Ube3a* allele (i.e., *Ube3a*$^{m+/FLOX}$ or *Ube3a*$^{m+/STOP}$) to heterozygous males from one of three *Cre*-expressing lines: *Nestin-Cre* mice (RRID:IMSR_JAX:003771) (Tronche et al., 1999), *Gad2-Cre* mice (RRID:IMSR_JAX:010802), or *NEX-Cre* mice (Goebbels et al., 2006), which Klaus-Armin Nave generously provided.

We maintained *Nestin-Cre* and *NEX-Cre* mice on a congenic C57BL/6 background. We always bred *Nestin-Cre* males to congenic C57BL/6 *Ube3a*$^{m+/FLOX}$ females to yield congenic C57BL/6 experimental offspring. The same was true for *NEX-Cre* breeding with regard to generation of congenic C57BL/6 animals for histology, electrophysiology experiments, and *Ube3a*$^{FLOX/p+}$*::NEX-Cre* offspring for flurothyl seizure assays.

Gad2-Cre mice were initially generated as C57/129 hybrids (Taniguchi et al., 2011), which had been backcrossed at least 3 generations toward C57BL/6 prior to our acquiring them from JAX. We used *Gad2-Cre* males backcrossed at least 4 times onto C57BL/6 to breed mice for whole-cell electrophysiology and electron microscopy experiments, and at least 7 times onto C57BL/6 to breed for flurothyl seizure assays. For *in vivo* LFP recordings and audiogenic seizure experiments, we used *Gad2-Cre* breeder males backcrossed at least 5 generations back toward 129S2/SvPasCrl when bred to congenic 129S2/SvPasCrl *Ube3a*$^{m+/STOP}$ females and *Gad2-Cre* breeder males backcrossed at least 9 generations back toward 129S2/SvPasCrl when crossed to 5x 129-backcrossed *Ube3a*$^{m+/FLOX}$ females (see above).

To generate litters for AAV-Cre injections, we crossed *Ube3a*$^{m+/FLOX}$ females to male homozygous *Ai9*, tdTomato Cre-reporter mice (RRID:IMSR_JAX:007909), which were maintained on a congenic C57BL/6 background (Madisen et al., 2010). We generated constitutively maternal Ube3a-deficient mice (*Ube3a*$^{m-/p+}$) by breeding congenic C57BL/6 *Ube3a*$^{m+/p-}$ females (RRID:IMSR_JAX:016590) to congenic C57BL/6 wild type males (Jiang et al., 1998).

Adeno-Associated Virus (AAV) Injections

We cryoanesthetized P0-P1.5 mouse pups on wet ice for ~3 minutes before transferring them to a chilled stage equipped with a fiber optic light source to transilluminate the lateral ventricles. We used a 10 μl syringe with a 32-gauge, 0.4 inch-long sterile syringe needle (7803-04, Hamilton, Reno, NV) to bilaterally deliver 0.5 μL of purified AAV (4 x 10^{12} viral genomes/mL) to the lateral ventricles. We added fast green dye (1 mg/mL) to the virus solution to verify successful injections. This procedure resulted in ~4 x 10^{9} total viral genomes being injected per pup. We specifically used AAV vectors with the serotype 9 capsid, which were packaged at the UNC Viral Vector Core with self-complementary genomes containing a modified hybrid CMV enhancer/chicken b-actin (CBh) promoter driving a Cre expression cassette (Gray et al., 2011). Following injection, we warmed pups on an isothermal heating pad with home-cage nesting material before returning them *en masse* to their typical home cage environment.

Electrophysiology

Acute coronal slice preparation. We anesthetized P70-P90 mice with pentobarbital (40 mg/kg) and, after confirming the disappearance of corneal reflexes, transcardially perfused them with ice-cold dissection buffer (in mM: 87 NaCl, 2.5 KCl, 1.25 $NaH2PO_4$, 26 $NaHCO_3$, 75 sucrose, 10 dextrose, 1.3 ascorbic acid, 7 $MgCl_2$, and 0.5 $CaCl_2$) bubbled with 95% O_2 and 5% CO_2. We then dissected the visual cortices and prepared 350 μm-thick coronal slices using a VT1000S vibrating microtome (Leica, Buffalo Grove, IL). We allowed slices to recover for 20 minutes in a 35º C submersion chamber filled with oxygenated artificial cerebrospinal fluid (ACSF) (in mM; 124 NaCl, 3 KCl, 1.25 $NaH2PO_4$, 26 $NaHCO_3$, 1 $MgCl_2$, 2 $CaCl_2$, and 20 dextrose), which we supplemented with 1.25 mM ascorbic acid. We then transferred the recovery chamber to room temperature where slices remained for a minimum of 40 minutes prior to use (Philpot et al., 2003).

Miniature excitatory and inhibitory postsynaptic current (mEPSC and mIPSC) recording conditions. In order to pharmacologically block action potential firing, inhibitory neurotransmission, and to isolate

AMPA (α-Amino-3-hydroxy-5-methyl-4-isoxazolepropionic acid) receptor-mediated mEPSCs, we perfused slices with 30º C, oxygenated ACSF containing 1 μM tetrodotoxin (TTX), 50 μM picrotoxin, and 100 μM D,L-2-amino-5-phosphonopentanoic acid (APV), and we performed recordings holding at -70 mV. For mIPSC experiments, we utilized ACSF containing 1 μM TTX, 20 μM 6,7-dinitroquinoxaline-2,3-dione (DNQX), and 100 μM APV. For most mIPSC experiments, we voltage-clamped neurons at 0 mV to maximize the chloride driving force for our standard Cs-based internal solutions. However, in a subset of experiments, we also used the following high chloride internal solution to more easily resolve mIPSCs (in mM): 2 NaCl, 141 KCl, 1 $CaCl_2$, 10 EGTA, 2 Mg-ATP, 0.3 Na-GTP, 10 HEPES, 10 Na-phosphocreatine, and 0.025 Alexa-594 with pH adjusted to 7.25 and osmolarity adjusted to ~295 mOsm with sucrose. We held neurons at -80 mV when using this internal.

Evoked inhibitory postsynaptic current (eIPSC) recording conditions. We recorded eIPSCs under identical conditions to those described for mIPSC experiments utilizing the Cs-based internal solution and a 0 mV holding potential, except that we withheld TTX from the ACSF to enable action potential firing. We electrically evoked IPSCs using a concentric bipolar stimulating electrode (200 μm tip separation) placed ~150 μm ventral to the recorded pyramidal neuron in L2/3. The duration of each electrical stimulus was 200 μs.

Evoked excitatory postsynaptic current (eEPSC) recording conditions. We recorded eEPSCs under identical conditions to those described for mEPSC experiments with two notable exceptions: 1) we excluded TTX and picrotoxin from the ACSF, and 2) we voltage clamped neurons at ~-45 mV (the empirically determined chloride reversal potential without adjusting for junction potential). Following the completion of excitatory synaptic depletion and recovery experiments we washed on DNQX and APV to confirm we were holding at the reversal potential for chloride; we excluded neurons from analysis if their eEPSC amplitude did not decrease to at least 20% of the recovery plateau. We performed electrical stimulation as described for eIPSC recordings.

Tonic inhibitory current recording conditions. We recorded δ-$GABA_AR$-mediated tonic currents in ACSF containing 20 μM DNQX and 100 μM APV while voltage clamping at -70 mV using a CsCl internal solution (in mM: 135 CsCl, 2.5 $MgCl_2$, 10 HEPES, 4 NaATP, 0.4 NaGTP, 10 NaCreatine, 0.6 EGTA, and 0.025 Alexa-594 with pH adjusted to 7.25 and osmolarity adjusted to ~295 mOsm with sucrose). We activated δ-$GABA_AR$-selective currents via bath application of 1 μM 4,5,6,7-Tetrahydroisoxazolo[5,4-*c*]pyridin-3-ol hydrochloride (THIP/Gaboxadol) for 10 minutes, chased for 10 minutes with 20 μM 6-Imino-3-(4-methoxyphenyl)-1(6*H*)-pyridazinebutanoic acid hydrobromide (SR95531/Gabazine), a pan-$GABA_AR$ competitive antagonist. We quantified δ-$GABA_AR$-mediated currents both by measuring the inward shift in the holding current ($I_{holding}$) following wash-on of THIP (mean $I_{holding}$ from last 2 minutes of THIP wash-on – mean $I_{holding}$ from last 2 minutes of a 5 minute baseline period) and by measuring the subsequent outward shift in $I_{holding}$ following Gabazine chase (mean $I_{holding}$ from last 2 minutes of Gabazine wash-on – mean $I_{holding}$ from last 2 minutes of THIP wash-on). We normalized changes in $I_{holding}$ to the membrane capacitance (Cm = Tm/Rm) of each cell. We measured Tm from a double-exponential fit to the decay phase (peak + 15 ms) of membrane capacitive transients evoked by -5 mV steps in the holding potential. We used the formula Tm = (A1/(A1+A2))*T1) + ((A2/(A1+A2))*T2), where A refers to the amplitude and T refers to the decay time constant of the two exponentials.

Behavioral Seizures

Flurothyl-induced seizures. We performed flurothyl (bis(2,2,2-trifluoroethyl) ether) seizure experiments in a ventilated chemical hood, testing mice individually within an air-tight glass chamber (~ 2 L in volume). We allowed mice to habituate to the chamber for 1 minute prior to the administration of 10% flurothyl in 95% ethanol, which we infused through a 5ml syringe onto a gauze pad suspended at the top of the chamber at a rate of 200 μl/min. We recorded resultant seizure behaviors using a video camera and scored the following events blind to genotype: 1) latency to the first myoclonic jerk (i.e., brief, but severe, contractions of the neck and body musculature occurring

while the mouse maintains postural control); 2) latency to the first generalized seizure (i.e., convulsions resulting in a loss of postural control). Upon observation of a generalized seizure, we immediately removed the lid of the chamber, exposing the mouse to fresh air, thereby facilitating cessation of the seizure. We cleaned the chamber with 70% ethanol and replaced the gauze pad between trials.

Audiogenic Seizures. We modeled our audiogenic seizure experiments after those described in a previous study (Michalon et al., 2012). We tested P70-P100 mice that were backcrossed 6-7 generations onto the 129S2/SvPasCrl background to enhance the penetrance of audiogenic seizure phenotypes. Following 1 minute of habituation to the behavioral chamber, we exposed mice to 30 seconds of loud sound (~125 dB) emitted by two simultaneously triggered personal alarm sirens (49-1010, RadioShack, Fort Worth, TX). We video-recorded each session and scored seizure severity blind to genotype.

qRT-PCR

For quantitative reverse transcriptase polymerase chain reaction (qRT–PCR) analysis, we extracted total RNA from the neocortices of ~P60 mice using Invitrogen TRIzol reagent (Life Technologies, Grand Island, NY). We then performed first strand cDNA synthesis on 500 ng–2 µg total RNA per sample using Invitrogen Superscript III reverse transcriptase (Life Technologies) primed with random hexamers. We used Invitrogen SYBR green (Life Technologies) for all qPCR reactions, which were run on a Rotorgene 3000 (Corbett Research, Sydney, Australia). We generated standard curves and C_t values using Rotorgene analysis software version 6.0, and we determined expression of *Ube3a* after normalization of each complementary DNA sample to expression levels of the housekeeping gene *Rpl22*. Primers were as follows: *Ube3a* F (5′-CAAAAGGTGCATCTAACAACTCA-3′), *Ube3a* R (5′-GGGGAATAATCCTCACTCTCTC-3′), *Rpl22* F (5′- AAGAAGCAGGTTTTGAAG-3′), and *Rpl22* R (5′-TGAAGTGACAGTGATCTTG-3′).

Western Blotting

We anesthetized mice with sodium pentobarbital (40 mg/kg i.p.) prior to decapitation and brain removal. We then rapidly dissected the neocortical hemispheres in ice-cold PBS, snap-froze them with liquid nitrogen, and stored them at -80°C. Using a glass tissue homogenizer (Wheaton, Millville, NJ), we homogenized frozen tissue samples with ice-cold RIPA buffer (50 mM Tris pH 8.0, 150 mM NaCl, 1% triton x-100, 0.1% SDS, 0.5% Na Deoxycholate) supplemented with 2 mM EDTA and a protease inhibitor cocktail (Sigma, Saint Louis, MO). We cleared homogenates via 16,000 x g centrifugation for 20 minutes at 4°C and we determined protein concentrations of the supernatants using the BCA assay (Thermo Scientific, Waltham, MA). Next, we resolved protein samples (30 µg per lane) by SDS-PAGE and transferred them to nitrocellulose membranes. We blocked membranes for 1 hour at room temperature in Odyssey blocking buffer (Li-COR, Lincoln, NE) prior to incubation overnight at 4°C with primary antibodies diluted in a 1:1 solution of blocking buffer and Tris-buffered saline containing 0.1% Tween-20 (TBST). We used the following primary antibodies: 1:1,000 mouse anti-UBE3A (Sigma-Aldrich Cat# E8655, RRID:AB_261956) and 1:5,000 mouse anti-GAPDH (Millipore Cat# MAB374, RRID:AB_2107445). We subsequently washed membranes with TBST prior to incubation for 1 hour at room temperature with donkey anti-mouse 800CW (LI-COR Biosciences Cat# 926-32212, RRID:AB_621847) diluted 1:10,000 in the same diluent as the primary antibodies. Finally, we repeatedly washed blots in TBST followed by TBS alone prior to imaging with the Odyssey imaging system (LI-COR).

Immunohistochemistry

For Light Microscopy. We anesthetized mice with sodium pentobarbital (40 mg/kg) prior to transcardial perfusion with phosphate-buffered saline (PBS), immediately followed by phosphate-buffered 4% paraformaldehyde (pH 7.3). We removed perfused brains from their skulls and postfixed them overnight at 4°C prior to sequential 12-hour incubations in 10%, 20%, and 30% sucrose in PBS (pH 7.5) for cryoprotection. We then froze cryoprotected brains on dry ice and cut them into 40 µm-

thick sections with a sliding microtome (Thermo Scientific). We stored sections at -20°C in a cryopreservative solution (by volume: 45% PBS, 30% ethylene glycol, 25% glycerol) until free-floating immunohistochemical processing.

For immunofluorescent staining, we rinsed sections several times in PBS before blocking in PBS plus 5% normal goat serum and 0.02% Triton-X-100 (NGST) for 1 hour at room temperature. We subsequently incubated blocked tissue sections in primary antibodies diluted in NGST for 48 hours at 4°C. We then rinsed them several times in PBS containing 0.02% Triton-X-100 (PBST) before incubation in secondary antibodies (also diluted in NGST) for 1 hour at room temperature. Primary antibodies used: 1:1,000 mouse anti-UBE3A (Sigma-Aldrich Cat# SAB1404508, RRID:AB_10740376), 1:500 mouse anti-NeuN (Millipore Cat# MAB377, RRID:AB_10048713), 1:2,000 mouse anti-parvalbumin (235, Swant, Marly, Switzerland), 1:500 rabbit anti-parvalbumin (PV-25, Swant), 1:1,000 rabbit anti-calretinin (7699/4, Swant), 1:500 rat anti-somatostatin (Millipore Cat# MAB354, RRID:AB_2255365), 1:1,000 rabbit anti-somatostatin (Bachem Cat# T-4103.0050, RRID:AB_518614), and 1:500 rabbit anti-Cux1 (Santa Cruz Biotechnology Cat# sc-13024, RRID:AB_2261231). We used secondary antibodies (Thermo Fisher Scientific) at a 1:500 dilution, including Alexa-488 goat anti-mouse IgG_{2a} (Cat# A21131, RRID:AB_10562578), Alexa-647 goat anti-mouse IgG_1 (Cat# A21240, RRID:AB_10565021), Alexa-568 goat anti-mouse IgG_1 (Cat# A21124, RRID:AB_10562737), Alexa-633 goat anti-mouse IgG (Cat# A21052, RRID:AB_10584496), Alexa-488 goat anti-rabbit IgG (Cat# A11008, RRID:AB_10563748), Alexa-568 goat anti-rabbit IgG (Cat# A11011, RRID:AB_10584650), Alexa-633 goat anti-rabbit IgG (Cat# A21070, RRID:AB_10562894), and Alexa-568 goat anti-rat IgG (Cat# A11077, RRID:AB_10562719). We stained all brain sections compared within figures in the same experiment, under identical conditions.

For Electron Microscopy. We anesthetized mice with sodium pentobarbital (40 mg/kg) prior to transcardial perfusion with 0.9% saline solution for 1 min, followed by a mixture of depolymerized 2% paraformaldehyde and 2% glutaraldehyde (Electron Microscopy Science, Hatfield, PA) in 0.1 M

phosphate buffer, pH 6.8. We then postfixed brains overnight in the same fixative before preparing 50 µm-thick sections on a vibratome. Next, we incubated vibratome sections in 1% osmium tetroxide in 0.1 M phosphate buffer (pH 6.8), followed by rinsing in 0.1 M maleate buffer (pH 6.0), before incubation in 1% uranyl acetate in maleate. We then dehydrated the sections in ethanol, infiltrated them with Spurr resin, and flat-embedded them between sheets of ACLAR plastic to create wafers, which we heat-polymerized. We cut chips of tissue from the wafers and glued them to plastic blocks to support the cutting of ~70 nm-thick sections, which we collected on copper mesh grids and poststained with uranyl acetate and Sato's lead.

We performed postembedding immunocytochemistry as previously described (Phend et al., 1992). Briefly, we pre-treated grids by incubating them at 60°C in 0.01M citrate buffer (pH 6.0) for 15 mins before blocking with 1% bovine serum albumin in Tris-buffered saline with 0.005% Tergitol NP-10 (TBSN, pH 7.6). We then incubated the grids overnight at 21–24 °C in rabbit anti-GABA antibody (Sigma-Aldrich Cat# A2052, RRID:AB_477652), diluted 1:100,000. Grids were rinsed, blocked in 1% normal goat serum in TBSN (pH 8.2), and incubated for 2 hours in goat anti-rabbit antibodies conjugated to 20 nm gold particles (EM.GAR20, BBI Solutions, Madison, WI). Finally, we rinsed the stained grids and then counterstained them with 1% uranyl acetate followed by Sato's lead.

Imaging and Figure Production

We acquired images of immunofluorescently stained brain sections with a Zeiss LSM 710 confocal microscope equipped with ZEN imaging Software (Zeiss, Jena, Germany, RRID:SCR_013672). We collected images compared within figures during the same imaging session using identical acquisition parameters. We collected all electron micrographs with a Tecnai electron microscope (Phillips, Andover, MA) at 80 KV. Occasionally, images were linearly adjusted for brightness and contrast using Image J software (RRID:SCR_003070) (Schneider et al., 2012). All images to be quantitatively compared underwent identical manipulations. We prepared all figures using Adobe Illustrator software (Adobe Systems Inc., San Jose, CA, RRID:SCR_010279).

Quantification of Neuron Density and Cre Recombination Efficiency

We acquired all images to be analyzed for interneuron density or Cre recombination efficiency using thin (1.4 μm-thick) optical sectioning. We quantified PV^+, CRT^+, and SOM^+ interneuron density from 5 strips (500 μm-wide) of primary visual cortex per mouse imaged at ~P80. We determined the efficiency of AAV-Cre-mediated deletion of maternal *Ube3a* by analyzing UBE3A colocalization in $tdTomato^+$ cells from 800 μm-wide strips of primary visual cortex imaged from P12 mice. We analyzed a total of 246 tdTomato+ cells from *Ube3a*$^{m+/p+}$ mice (5 images) and 337 $tdTomato^+$ cells from *Ube3a*$^{FLOX/p+}$ mice (10 images).

Statistical Analyses

Composition of experimental "Control" groups:

Figures S3, S4, and S7: *Ube3a*$^{m+/p+}$ and *Ube3a*$^{m+/p+}$*::Nestin-Cre*.

Figures 1, 4D, 5C, 5D, 6B, 7A, S2, and S8A-C: *Ube3a*$^{m+/p+}$, *Ube3a*$^{FLOX/p+}$, and *Ube3a*$^{m+/p+}$*::Gad2-Cre*.

Figures 3E-G, and 4C: *Ube3a*$^{m+/p+}$, *Ube3a*$^{FLOX/p+}$, and *Ube3a*$^{m+/p+}$*::NEX-Cre*.

Figures 2, 5B, 6C, 7B, S5, and S8D-F: *Ube3a*$^{m+/p+}$ and *Ube3a*$^{m+/p+}$*::Gad2-Cre*.

Figure 3C: *Ube3a*$^{m+/p+}$ and *Ube3a*$^{m+/p+}$*::NEX-Cre*.

Statistical analyses by experiment:

Interneuron density: 2-way ANOVA with Sidak's (Figure S2A) or Tukey's (Figure S4A) post-hoc test.

AAV-Cre-mediated recombination efficiency: Unpaired, 2-tailed student's t-test (Figure $S6A_4$).

mIPSCs and mEPSCs: 1-way ANOVA with Tukey's post-hoc test (Figures S4B, S4C, and S5A-C) and unpaired, 2-tailed student's t-test (Figures 1C, 3F, and S2B).

Paired-pulse: Kruskal-Wallis test (Figure S4E), 1-way ANOVA with Tukey's post-hoc test (Figure S5D) and unpaired, 2-tailed student's t-test (Figure S2C).

Input-output: 2-way repeated measures ANOVA with either Tukey's (Figures 2C, 3C, S4D and S6B) or Sidak's (Figures 1D and 3E) post-hoc test.

Recovery from high-frequency synaptic depletion: 1-way ANOVA with Tukey's post-hoc test (Figures 2D, S4F, and S5E) or unpaired, 2-tailed student's t-test (Figure 1E), each comparing the last 108 seconds of the recovery phase.

Flurothyl-induced seizures: Unpaired, 2-tailed student's t-test (Figure 4C and $4D_1$-D_2).

Flurothyl survival: Log-rank (Mantel-Cox) test (Figure $4D_3$).

Post-weaning lethality: Chi-square test (Figure 5D).

Audiogenic seizures: Chi-square test (Figure 5B and 5C).

LFP spectral power: Unpaired, 2-tailed student's t-test (Figure $6B_3$) or 1-way ANOVA with Tukey's post-hoc test (Figure $6C_3$) of delta power band.

Ultrastructural analyses of presynaptic terminals: Unpaired, 2-tailed student's t-test (Figures $7A_3$-A_5 and S8A-C) or 1-way ANOVA with Tukey's post-hoc test (Figures $7B_4$-B_6, S7B-D, and S8D-F).

SUPPLEMENTAL REFERENCES

Berrios, J., Stamatakis, A.M., Kantak, P.A., McElligott, Z.A., Judson, M.C., Aita, M., Rougie, M., Stuber, G.D., and Philpot, B.D. (2016). Loss of UBE3A from TH-expressing neurons suppresses GABA co-release and enhances VTA-NAc optical self-stimulation. Nat Commun *7*, 10702.

Goebbels, S., Bormuth, I., Bode, U., Hermanson, O., Schwab, M.H., and Nave, K.A. (2006). Genetic targeting of principal neurons in neocortex and hippocampus of NEX-Cre mice. Genesis *44*, 611-621.

Gray, S.J., Foti, S.B., Schwartz, J.W., Bachaboina, L., Taylor-Blake, B., Coleman, J., Ehlers, M.D., Zylka, M.J., McCown, T.J., and Samulski, R.J. (2011). Optimizing promoters for recombinant adeno-associated virus-mediated gene expression in the peripheral and central nervous system using self-complementary vectors. Hum Gene Ther *22*, 1143-1153.

Jiang, Y.H., Armstrong, D., Albrecht, U., Atkins, C.M., Noebels, J.L., Eichele, G., Sweatt, J.D., and Beaudet, A.L. (1998). Mutation of the Angelman ubiquitin ligase in mice causes increased cytoplasmic p53 and deficits of contextual learning and long-term potentiation. Neuron *21*, 799-811.

Madisen, L., Zwingman, T.A., Sunkin, S.M., Oh, S.W., Zariwala, H.A., Gu, H., Ng, L.L., Palmiter, R.D., Hawrylycz, M.J., Jones, A.R.*, et al.* (2010). A robust and high-throughput Cre reporting and characterization system for the whole mouse brain. Nat Neurosci *13*, 133-140.

Michalon, A., Sidorov, M., Ballard, T.M., Ozmen, L., Spooren, W., Wettstein, J.G., Jaeschke, G., Bear, M.F., and Lindemann, L. (2012). Chronic pharmacological mGlu5 inhibition corrects fragile X in adult mice. Neuron *74*, 49-56.

Phend, K.D., Weinberg, R.J., and Rustioni, A. (1992). Techniques to optimize post-embedding single and double staining for amino acid neurotransmitters. J Histochem Cytochem *40*, 1011-1020.

Philpot, B.D., Espinosa, J.S., and Bear, M.F. (2003). Evidence for altered NMDA receptor function as a basis for metaplasticity in visual cortex. J Neurosci *23*, 5583-5588.

Schneider, C.A., Rasband, W.S., and Eliceiri, K.W. (2012). NIH Image to ImageJ: 25 years of image analysis. Nat Methods *9*, 671-675.

Silva-Santos, S., van Woerden, G.M., Bruinsma, C.F., Mientjes, E., Jolfaei, M.A., Distel, B., Kushner, S.A., and Elgersma, Y. (2015). Ube3a reinstatement identifies distinct developmental windows in a murine Angelman syndrome model. J Clin Invest *125*, 2069-2076.

Taniguchi, H., He, M., Wu, P., Kim, S., Paik, R., Sugino, K., Kvitsiani, D., Fu, Y., Lu, J., Lin, Y.*, et al.* (2011). A resource of Cre driver lines for genetic targeting of GABAergic neurons in cerebral cortex. Neuron *71*, 995-1013.

Tronche, F., Kellendonk, C., Kretz, O., Gass, P., Anlag, K., Orban, P.C., Bock, R., Klein, R., and Schutz, G. (1999). Disruption of the glucocorticoid receptor gene in the nervous system results in reduced anxiety. Nat Genet *23*, 99-103.